

Published in IET Control Theory and Applications
 Received on 8th June 2007
 Revised on 4th January 2008
 doi: 10.1049/iet-cta:20070195



ISSN 1751-8644

Discrete-time bilateral teleoperation: modelling and stability analysis

M. Tavakoli¹ A. Aziminejad^{2,3} R.V. Patel^{2,3} M. Moallem⁴

¹School of Engineering and Applied Sciences, Harvard University, 60 Oxford Street, Cambridge, MA 02138, USA

²Department of Electrical and Computer Engineering, University of Western Ontario, London, ON, Canada N6A 5B9

³Canadian Surgical Technologies and Advanced Robotics (CSTAR), 339 Windermere Road, London, ON, Canada N6A 5A5

⁴School of Engineering Science, Simon Fraser University, Burnaby, BC, Canada V5A 1S6

E-mail: tavakoli@seas.harvard.edu

Abstract: Discretisation of a stabilising continuous-time bilateral teleoperation controller for digital implementation may not necessarily lead to stable teleoperation. While previous research has focused on the question of passivity or stability of haptic interaction with a discretely simulated virtual wall, here the stability of master–slave teleoperation under discrete-time bilateral control is addressed. Stability regions are determined in the form of conditions involving the sampling period, control gains including the damping introduced by the controller and environment stiffness. Among the obtained stability conditions are lower and upper bounds on the controller damping in addition to upper bounds on the sampling period and the environment stiffness, implying that as the sampling period is increased, the maximum admissible stiffness of the environment with which a slave robot can stably interact is reduced. An outcome of the paper is a set of design guidelines in terms of selection of various control parameters and the sampling rate for stable teleoperation under discrete-time control. Because of the sampling period–environment stiffness tradeoff and the stability–transparency tradeoff, the obtained stability boundaries are of particular importance for hard-contact teleoperation or when the teleoperation system has near-ideal or ideal transparency. The results of the stability analysis are confirmed by a simulation study in which the bilateral controller is realised by z-domain transfer functions while the master, the slave and the environment are simulated in the s-domain.

Nomenclature

α	ratio of $C_m(s)$ to $C_s(s)$	$f_c(t)$	slave/environment interaction
Δ_j	determinant for Routh–Hurwitz test	$f_h(t)$	hand/master interaction
γ_1	lower bound on k_e	$f_m(t)$	master control signal
γ_2	upper bound on k_e	$f_s(t)$	slave control signal
$\tilde{f}_e(t)$	environment's exogenous input force	$G_{h0}(s)$	zero-order hold
$\tilde{f}_h(t)$	operator's exogenous input force	$H(s)$	hybrid matrix
b	haptic interface damping	$h_{ij}(s)$	hybrid matrix element
b_w	virtual wall damping	k_e	environment stiffness
C_1, \dots, C_6	bilateral control gains	k_w	virtual wall stiffness
$C_m(s)$	master's PD controller	k_{p_m}	proportional gain of $C_m(s)$
$C_s(s)$	slave's PD controller	k_{p_s}	proportional gain of $C_s(s)$
$f^*(t)$	sampled-data $f(t)$	k_{v_m}	derivative gain of $C_m(s)$
		k_{v_s}	derivative gain of $C_s(s)$
		M_m	master inertia

M_s	slave inertia
$S(s)$	scattering matrix
T	sampling period
V_3	third-order Verlet approximation
V_5	fifth-order Verlet approximation
$x_m(t)$	master position
$x_s(t)$	slave position
$Z_c(s)$	remote environment's impedance
$Z_h(s)$	operator hand's impedance
$Z_m(s)$	master impedance
$Z_s(s)$	slave impedance
$Z_t(s)$	impedance transmitted to the operator

1 Introduction

In bilateral master–slave operation, a user operates from and receives feedback of slave/environment interactions via a master interface while a slave robot mimics the user's hand manoeuvres on the remote environment. Besides stability which is the primary requisite for safe teleoperation, the ideal performance goal is that the combination of the master, the slave and the bilateral controller is 'transparent', implying that the dynamics of the environment is displayed to the user with no distortion. For achieving stable and possibly transparent teleoperation, various teleoperation control architectures are proposed and used in the literature [1–3] including position-error-based (PEB) control, direct force reflection (DFR) control and four-channel control. The four-channel bilateral teleoperation method is the most comprehensive architecture, as it can represent other teleoperation methods through appropriate selection of its control parameters. It is also the most flexible method because, unlike other methods, it can guarantee ideal transparency.

The stability and/or transparency of a teleoperation system can be jeopardised due to non-idealities which exist in practice and are often not considered during control design. Among the effects studied so far are master–slave communication delays [4–6] including variable delays in Internet-based teleoperation [7], contact transition [8] and friction [9].

Another detriment to teleoperation stability and transparency, whose importance warrants a separate analysis, is sampling during discrete-time implementation of bilateral controllers. Problems with teleoperation stability arise when a bilateral controller designed in the continuous-time domain is converted into the discrete-time domain for implementation as a digital controller. Because of the wealth of continuous-time design methods, discretising predesigned continuous-time controllers rather than direct discrete-time design is very common and, in teleoperation control, overwhelmingly the method of

choice. In this approach, the sampling frequency is chosen based on the continuous-time closed-loop bandwidth, which is available from the knowledge of the analogue control system. As will be seen in this paper, such a system may become unstable particularly when the slave robot is interacting with a stiff environment or when the teleoperation system has near-ideal or ideal transparency (which corresponds to a small stability margin).

With passivity being a sufficient condition for stability of a system terminated to other passive elements, previous research has investigated the passivity of a communication channel over a sampled data, packet-switched network such as the Internet in the face of varying delay and packet loss [10, 11]. Since a zero-order hold (ZOH) creates energy leaks that can make an otherwise passive system non-passive [12], some researchers have studied the effect of sampled-data control on system passivity. Leung and Francis [13] found that the discrete-time counterpart of a continuous-time stabilising bilateral controller may not necessarily stabilise the teleoperator, but the sampled-data system could be stabilised for sufficiently small sampling periods by using six low-pass filters. To address the problem of passivity-preserving sampling, Anderson [14] proposed to model a control system as a cascade of passive scattering modules and discretise each module using Tustin's method, which has been shown to maintain the passivity of a passive scattering operator. On the basis of port-Hamiltonian systems framework, sampling in a way that passivity is preserved is investigated by Secchi *et al.* [15] and Stramigioli *et al.* [16].

For the specific problem of haptic rendering of a discretely simulated virtual wall, Colgate and Schenkel [17] found the necessary and sufficient conditions for passivity of the virtual wall as

$$b > \frac{k_w T}{2} + b_w \quad (1)$$

where $b > 0$ is the haptic interface damping and $k_w > 0$ and $b_w > 0$ are the virtual wall stiffness and damping, respectively. It is confirmed by (1) that passivity competes with transparency, which requires high k_w and b_w . Colgate and Schenkel attempted to avoid explicit modelling of human operator's dynamics by establishing the passivity of the haptic display (haptic device, virtual coupling and virtual environment). Miller *et al.* [18] extended this basic approach to haptic systems incorporating a broad class of nonlinear time-delayed virtual environments. In a general nonlinear regime, they introduced the concept of cyclo-passivity in order to mitigate the intrinsic restrictions of the problem. Moreover, their extension included non-passive virtual environments and guidelines were provided to design nonlinear virtual environments to ensure the absence of oscillation and other chaotic behaviour in the signal presented to the human operator. Mahvash and Hayward extended the above result to nonlinear multidimensional virtual environments and nonlinear devices [19]. On the

other hand, Abbott and Okamura [20] found an upper bound on the virtual wall stiffness as a function of the sampling rate, encoder resolution and friction in order to ensure virtual wall passivity. Diolaiti *et al.* [21] analysed how Coulomb friction allows a haptic interface that is in violation of passivity conditions during interaction with a virtual wall to operate stably.

Rather than passivity, Love and Book [22] directly studied the stability of haptic rendering of a discretely simulated virtual wall by applying Jury stability criterion. Also, Gil *et al.* [23, 24] applied the Routh Hurwitz criterion to the characteristic equation of the system to obtain a necessary and sufficient condition for stability that can be approximated by

$$b > \frac{k_w T}{2} - b_w \quad (2)$$

Evidently, the stability condition (2) is less conservative than the passivity condition (1) and allows for higher transparency. Moreover, both the haptic interface damping b and the virtual wall damping b_w help to achieve stability with longer sampling periods and for stiffer environments. Although the above indicates that the stiffness that can be rendered by a haptic interface is upper bounded by the sampling frequency, in practice an excessive increase in sampling frequency can push vibration frequencies into ranges more easily perceptible by the sense of touch [25]. On the other hand, Shen and Goldfarb [26] proposed to use pneumatic actuation in a haptic interface to increase the open-loop stiffness, thus enhancing the range of achievable closed-loop stiffnesses compared with electric motor actuation.

While research so far has focused on the passivity or stability of haptic interaction with a discretely simulated virtual wall, this paper for the first time addresses the stability of master–slave teleoperation when the bilateral controller is implemented in discrete-time using constant sampling periods. The contributions of this paper are as follows. First, considering the general four-channel bilateral teleoperation architecture, which can represent other teleoperation methods including PEB and DFR control

through appropriate selection of its control gains, we derive a hybrid model of the digitally controlled teleoperation system. Using this model and without making any assumption about the human operator dynamics (by modelling the operator as an exogenous input force), regions of stability of the discrete-time controlled teleoperation system are obtained in the form of conditions involving the sampling period, the environment stiffness and the control parameters including the controller damping. Specifically, requirements on the control parameters and the sampling period are found such that stability is ensured when the slave is in free space. For the case that the slave is in contact with an environment, stability conditions are derived in the form of lower and upper bounds on the controller damping in addition to upper bounds on the sampling period and the environment stiffness. An outcome of the paper is a set of design guidelines in terms of selection of various control parameters and the sampling rate for stable bilateral teleoperation under discrete-time control. The obtained stability boundaries are of particular importance for teleoperation on a rigid environment or when the teleoperation system has near-ideal or ideal transparency. We confirm our theoretical results by a simulation study containing a z -domain bilateral controller and s -domain master, slave and environment models.

2 Teleoperation stability analysis tools

The block diagram of a bilateral master–slave system is shown in Fig. 1. Here, $\tilde{f}_h(t)$ and $\tilde{f}_e(t)$ are, respectively, the operator's and the environment's exogenous input forces and are independent of the teleoperation system behaviour. The hand/master and the slave/environment interactions (force or torque) are denoted by $f_h(t)$ and $f_e(t)$, respectively. The master and the slave positions and control signals (force or torque) are shown by $x_m(t)$, $x_s(t)$, $f_m(t)$ and $f_s(t)$, respectively. The impedances $Z_h(s)$, $Z_e(s)$, $Z_m(s)$ and $Z_s(s)$ denote the dynamic characteristics of the human operator's hand, the remote environment, the master robot and the slave robot, respectively. The impedance $Z_t(s)$ is the perception of the user about the environment impedance

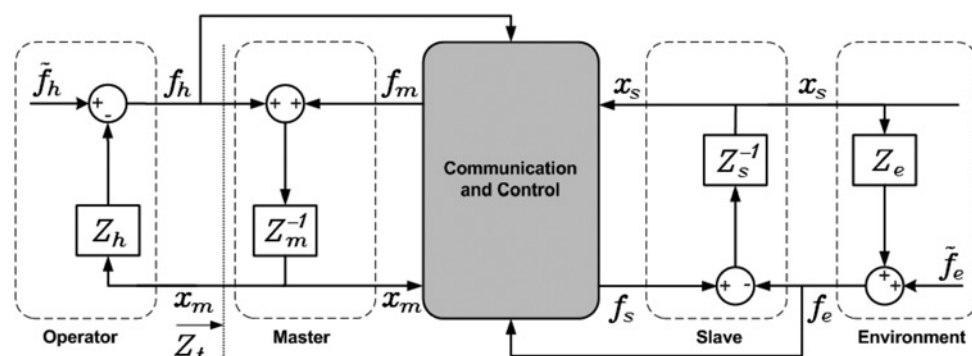


Figure 1 Block diagram of a master–slave teleoperation system

$Z_e(s)$. As shown in Fig. 1, the dynamics of the master and the slave can be written in the frequency domain as

$$\begin{aligned} F_m + F_h &= Z_m X_m = M_m s^2 X_m \\ F_s - F_e &= Z_s X_s = M_s s^2 X_s \end{aligned} \quad (3)$$

where M_m and M_s are the master and the slave inertias, respectively. If the master and slave impedances included damping terms, in continuous-time, they would contribute to the closed-loop equations in the same way as the derivative terms of the master and slave PD controllers (C_m and C_s in Section 3). When the PD controllers are discretised, however, the robot and controller damping terms can no longer be dumped together, resulting in mathematical complexities in our stability analysis. Therefore we assume no damping for the master or the slave.

The teleoperation system of Fig. 1 can be modelled as a two-port network with the following hybrid matrix representation

$$\begin{bmatrix} F_h \\ -X_s \end{bmatrix} = \begin{bmatrix} b_{11}(s) & b_{12}(s) \\ b_{21}(s) & b_{22}(s) \end{bmatrix} \begin{bmatrix} X_m \\ F_e \end{bmatrix} \quad (4)$$

Each element of the H matrix has a physical meaning. The hybrid parameter $b_{11} = F_h/X_m|_{F_e=0}$ is the input impedance in free-motion condition. Non-zero values for b_{11} mean that even when the slave is in free space, the user will receive some force feedback, thus giving a 'sticky' feel of free-motion movements. The parameter $b_{12} = F_h/F_e|_{X_m=0}$ is a measure of force tracking for the haptic teleoperation system when the master is locked in motion (perfect force tracking for $b_{12} = 1$). The parameter $b_{21} = -X_s/X_m|_{F_e=0}$ is a measure of position tracking performance when the slave is in free space (perfect position tracking for $b_{21} = -1$). The parameter $b_{22} = -X_s/F_e|_{X_m=0}$ is the output admittance when the master is locked in motion. Non-zero values for b_{22} indicate that even when the master is locked in place, the slave will move in response to slave/environment contacts.

For analysis of stability of a teleoperation system, the knowledge of the human operator and the environment dynamics are needed in addition to the teleoperation system model (4). Analysis of passivity, however, is independent of $Z_h(s)$ and $Z_e(s)$, and only assumes that the environment is passive ($\tilde{f}_e = 0$), and the operator is passive in the sense that he/she does not perform actions that will make the teleoperation system unstable. With passive but otherwise arbitrary terminations $Z_h(s)$ and $Z_e(s)$ and using Llewellyn's criterion or based on the singular values of the scattering matrix of the teleoperation system (Appendix 1), stability conditions independent of the human operator and the environment (absolute stability) may be derived. The scattering matrix $S(s)$ of a teleoperation system satisfies $F - X = S(s)(F + X)$ where $F = [F_h \ F_e]^T$ and $X = [X_m \ -X_s]^T$.

Analysis of stability based on Llewellyn's criterion or singular values of the scattering matrix is conservative as it ensures stability regardless of the teleoperation system's terminations (i.e. the human operator and the remote environment). Although it is useful to remove any assumption on the operator, the environment model can be incorporated into the analysis for less conservative stability regions. With the remote environment impedance Z_e , that is $F_e = Z_e X_s$ (for passivity reasons, $\tilde{f}_e = 0$), the general teleoperation system given by (4) has the following transfer function from F_h to X_m

$$\frac{X_m}{F_h} = \frac{1 + b_{22}Z_e}{b_{11}(1 + b_{22}Z_e) - b_{12}b_{21}Z_e} \quad (5)$$

Assuming that the environment is modelled by a linear spring, $Z_e = k_e$, the characteristic equation for the transfer function from F_h to X_m (and to any other output) is given by

$$b_{11}s + k_e(b_{11}b_{22} - b_{12}b_{21}) = 0 \quad (6)$$

The characteristic equation (6) must have no zeros in the right-half plane (RHP) for the teleoperation system to be stable regardless of the operator dynamics.

To remove any assumption on the human operator's impedance Z_h , we model the operator as an exogenous input force. In practice, the human operator with a finite impedance dynamic range relaxes the absolute stability conditions and improves the stability robustness [27]. Also note that we have assumed linear models in (3) and have neglected nonlinear terms such as friction and encoder quantisation. It is well known that friction plays a stabilising role in a teleoperation system. Indeed, it has been shown that Coulomb friction can dissipate the energy introduced by encoder quantisation [21, 20]. Therefore the stability analysis using linear models results in worst-case stability conditions [24].

3 Stability of a teleoperation system with continuous-time bilateral control

Fig. 2 depicts a general bilateral teleoperation architecture, in which position and force values are transmitted from the master to the slave and vice versa through four communication channels (4CH architecture) [1]. The compensators C_5 and C_6 in Fig. 2 constitute local force feedback at the slave and the master sides, respectively. The 4CH architecture can represent other teleoperation structures through appropriate selection of subsystem dynamics C_1 to C_6 . For instance, $C_1 = C_s$, $C_4 = -C_m$ and $C_2 = C_3 = C_5 = C_6 = 0$ amounts to PEB control and $C_1 = C_s$, $C_2 = 1$ and $C_3 = C_4 = C_5 = C_6 = C_m = 0$ leads to DFR control.

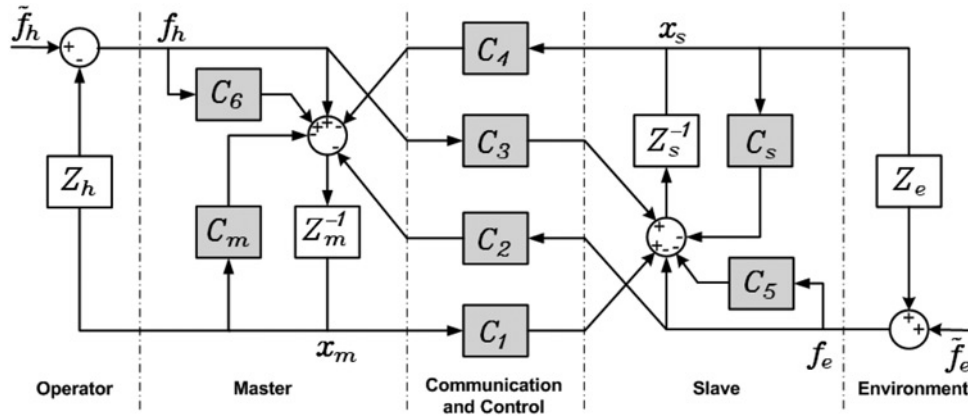


Figure 2 Four-channel bilateral teleoperation system
Shaded blocks represent control components

The controllers C_m and C_s are usually chosen as proportional-derivative controllers. Taking $C_m = k_{v_m}s + k_{p_m}$ and $C_s = k_{v_s}s + k_{p_s}$, as shown in [8] and Appendix 2, the PEB teleoperation architecture is absolutely stable if $k_{v_m}, k_{p_m}, k_{v_s}, k_{p_s} > 0$ and

$$\frac{C_m(s)}{C_s(s)} = \alpha \quad (7)$$

where α is a non-negative constant. Throughout this paper, we assume (7) in the general case of four-channel control. With DFR teleoperation, $\alpha = 0$.

In contrast to two-channel teleoperation architectures such as the PEB and the DFR methods, a sufficient number of parameters (degrees of freedom) in the 4CH architecture enables it to achieve ideal transparency (i.e. $x_m = x_s$ and $f_h = f_e$ regardless of the operator and environment dynamics). For ideal transparency, the hybrid matrix in (4) should be

$$H = \begin{bmatrix} 0 & 1 \\ -1 & 0 \end{bmatrix} \quad (8)$$

Equating the 4CH system hybrid parameters to (8) leads to the following teleoperation control design

$$C_1 = Z_{ts}, \quad C_2 = 1 + C_6, \quad C_3 = 1 + C_5, \quad C_4 = -Z_{tm} \quad (9)$$

By selecting the bilateral teleoperation controllers as in (9), the hybrid and scattering matrices of the 4CH teleoperation system become

$$H = \begin{bmatrix} 0 & \frac{D}{B} \\ -\frac{D}{B} & 0 \end{bmatrix}, \quad S = \begin{bmatrix} \frac{-D^2 + D^2}{2D^2} & \frac{2D^2}{2D^2} \\ \frac{2D^2}{2D^2} & \frac{D^2 - D^2}{2D^2} \end{bmatrix} \quad (10)$$

where $D = -C_3C_4 + Z_{ts}(1 + C_6)$, $Z_{tm} = Z_m + C_m$ and

$Z_{ts} = Z_s + C_s$. Using either Llewellyn's criterion or the scattering matrix condition (Appendix 1), the ideally transparent teleoperation system is stable iff D is RHP-analytic. If so, H simplifies to (8), and S is reduced to an off-diagonal, reciprocal matrix with both of its singular values equal to 1. Since under ideal transparency condition the system is reciprocal, according to Appendix 1, the stability of the system can be deduced.

As a result, under ideal transparent conditions, the teleoperation system stability critically depends on exact implementation of control laws because any departure from (9) risks violating (59) (i.e. a singular value may become larger than unity). Such a low stability margin for the ideally transparent teleoperator can be explained by the tradeoff that exists between stability and transparency in bilateral teleoperation [1]. Therefore it is important to investigate the effect of discrete-time control law implementation on the teleoperation system stability. It must be noted that although this research has been mainly motivated by the critical stability of an ideally transparent 4CH teleoperation system, in the stability analysis that follows we make no assumptions on C_2, C_3, C_5 or C_6 as was done in (9), in order to cover all teleoperation methods including PEB and DFR architectures.

4 Modelling of a teleoperation system with discrete-time bilateral control

The four-channel architecture of Fig. 2 under discrete-time control is shown in Fig. 3. As shown, the operator, the master, the slave and the environment remain continuous-time entities. For an input $f(t)$ to an ideal sampler starting at $t = 0$, the output is $f^*(t) = \sum_{k=0}^{\infty} f(kT)\delta(t - kT)$ where T is the sampling period. Since $z = e^{sT}$, the Laplace and Z transforms of the sampled-data signal $f^*(t)$ are $F^*(s) = \mathcal{L}[f^*(t)] = \sum_{k=0}^{\infty} f(kT)e^{-kTs}$ and $F(z) = \mathcal{Z}[f^*(t)] = F^*(s)|_{s=(1/T)\ln z}$. In Fig. 3, the two ZOH blocks reconstruct continuous-time control signals $f_m(t)$

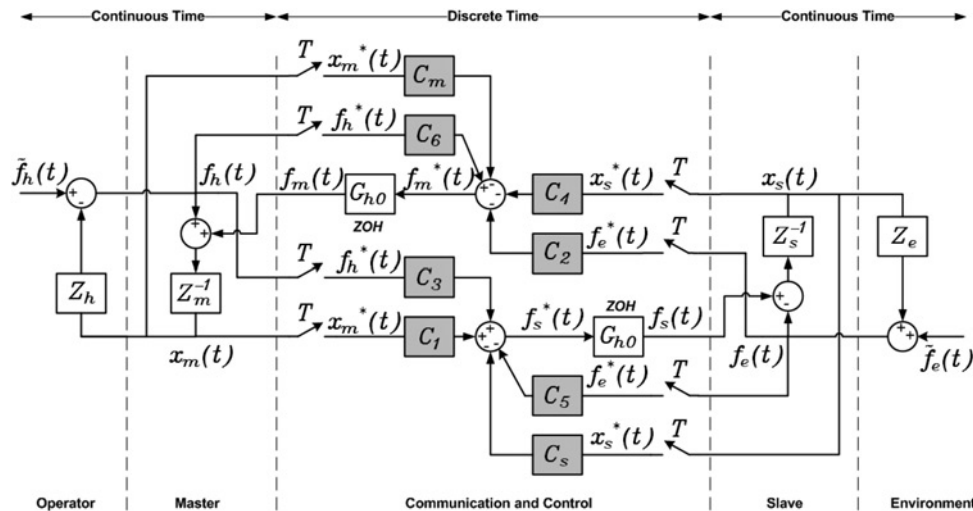


Figure 3 Digitally controlled four-channel bilateral teleoperation system

Shaded blocks represent control components

and $f_s(t)$ from discrete-time counterparts $f_m^*(t)$ and $f_s^*(t)$ via the following transfer function

$$G_{h0}(s) = \frac{1 - e^{-Ts}}{s} \quad (11)$$

With the four-channel structure shown in Fig. 3, since $C_m, C_s, C_1, \dots, C_6$ are all discrete-time controllers, the discrete-time control signals for the master and the slave can be written as

$$F_m^* = -C_m X_m^* - C_4 X_s^* + C_6 F_h^* - C_2 F_e^* \quad (12)$$

$$F_s^* = C_1 X_m^* - C_s X_s^* + C_3 F_h^* - C_5 F_e^*$$

Using (12) and substituting for $F_m = G_{h0} F_m^*$ and $F_s = G_{h0} F_s^*$ in (3), the closed-loop dynamics of the master and the slave in discrete-time are written as

$$X_m(z) = \mathcal{Z}[Z_m^{-1} F_h] + \mathcal{Z}[Z_m^{-1} G_{h0}](-C_m(z)X_m(z) - C_4(z)X_s(z) + C_6(z)F_h(z) - C_2(z)F_e(z)) \quad (13)$$

$$X_s(z) = -\mathcal{Z}[Z_s^{-1} F_e] + \mathcal{Z}[Z_s^{-1} G_{h0}](C_1(z)X_m(z) - C_s(z)X_s(z) + C_3(z)F_h(z) - C_5(z)F_e(z))$$

With $Z_m = M_m s^2$ and $Z_s = M_s s^2$, we have

$$\mathcal{Z}[Z_{m,s}^{-1} G_{h0}] = \frac{T^2}{2M_{m,s}} \frac{z+1}{(z-1)^2} \quad (14)$$

where, for brevity, commas in subscripts mean ‘or’ and present multiple equations. Using Tustin’s method, the PD controller C_s is discretized as $C_s = k_{v_s}(2(z-1)/(T(z+1))) + k_{p_s}$ and C_m is obtained from (7). Also, $C_1 = C_s$ and $C_4 = -\hat{C}_m$ are selected, which involve a slight departure from the ideal

transparent design (9) as the acceleration terms are neglected to reduce noise. At this stage, we make no assumptions on C_2, C_3, C_5 or C_6 in order to cover all teleoperation methods.

Note that in (13), $\mathcal{Z}[Z_m^{-1} F_h] \neq Z_m^{-1}(z)F_h(z)$ and $\mathcal{Z}[Z_s^{-1} F_e] \neq Z_s^{-1}(z)F_e(z)$ because the master and the slave transfer functions Z_m^{-1} and Z_s^{-1} operate in continuous time (i.e. F_h and F_e are not sampled). To be able to derive a hybrid model representation from (13), we need to approximate $\mathcal{Z}[Z_m^{-1} F_h]$ and $\mathcal{Z}[Z_s^{-1} F_e]$ by products of $F_h(z)$ and $F_e(z)$ given that Z_m^{-1} and Z_s^{-1} are double integrators.

Two Taylor series expansions of $g(t) = \int_0^t \int_0^s f(r) dr ds$ around the sampling instant kT are

$$g(kT \pm T) = g(kT) \pm Tg'(kT) + (T^2/2)g''(kT) \pm (T^3/6)g'''(kT) + \mathcal{O}(T^4) \quad (15)$$

Since $g''(kT) = f(kT)$, summing $g(kT + T)$ and $g(kT - T)$ and taking \mathcal{Z} transform on both sides gives the Verlet double integrator

$$G(z) = T^2 \frac{z}{(z-1)^2} F(z) = V_3(z)F(z) \quad (16)$$

which is an order more accurate than integration by the Euler method as third-order terms in the Taylor expansions cancel out. The double integration precision can be increased to $\mathcal{O}(T^6)$ where fifth-order terms cancel out:

$$G(z) = \frac{4T^2}{3} \frac{z(z^2 + z + 1)}{(z^2 - 1)^2} F(z) = V_5(z)F(z) \quad (17)$$

where the Tustin’s transformation $2(z-1)/(T(z+1))$ has replaced the derivative operator s .

On the basis of (16) and (17)

$$\mathcal{Z}[Z_{m,s}^{-1}F_{h,e}] = \frac{V_i(z)}{M_{m,s}}F_{h,e}(z), \quad i = 3, 5 \quad (18)$$

Replacing (14) and (18) in (13) gives the hybrid model of the digitally controlled teleoperation system as

$$\begin{bmatrix} F_h(z) \\ -X_s(z) \end{bmatrix} = \begin{bmatrix} b_{11}(z) & b_{12}(z) \\ b_{21}(z) & b_{22}(z) \end{bmatrix} \begin{bmatrix} X_m(z) \\ F_e(z) \end{bmatrix} \quad (19)$$

5 Stability of a teleoperation system with discrete-time bilateral control

Using the discrete-time hybrid parameters (19) in (6), the characteristic equation of the teleoperation system is obtained. The characteristic equation has ten roots on the unit circle irrespective of the system parameters, leaving for stability analysis a fourth- and an eighth-order polynomial in z when $i = 3$ and $i = 5$ in (18), respectively. To be able to apply the Routh–Hurwitz criterion to the simplified characteristic equation, we consider the r -transformation $z = (r + 1)/(r - 1)$ which maps the interior of the unit circle $|z| = 1$ onto the left half of the r -plane. The result is a fourth-order polynomial in r if $i = 3$ and a sixth-order polynomial in r (after factoring out r^2) if $i = 5$. To derive the stability requirements based on these characteristic equations, we frequently utilise the following basic facts.

- The polynomial $r^n + b_1r^{n-1} + \dots + b_n = 0$ is Hurwitz (i.e. its coefficients are positive real numbers and its zeros are located in the left half-plane of the complex plane) if and only if for $j = 1, \dots, n$

$$\Delta_j = \begin{vmatrix} b_1 & 1 & 0 & \dots & 0 \\ \vdots & \vdots & \vdots & \ddots & \vdots \\ b_{2j-1} & b_{2j-2} & b_{2j-3} & \dots & b_{2j} \end{vmatrix} > 0 \quad (20)$$

- The quadratic equation $ax^2 + bx + c = 0$ has two solutions x_1 and x_2 for which $x_1 + x_2 = -b/a$ and $x_1x_2 = c/a$. If $b^2 - 4ac < 0$ (two complex conjugate roots), the expression $ax^2 + bx + c$ has the same sign as a regardless of x . If $b^2 - 4ac \geq 0$ (two real roots), $ax^2 + bx + c$ has the same sign as a only for $x < \min\{x_1, x_2\}$ or $x > \max\{x_1, x_2\}$. Moreover, the two real roots will have the same sign if $c/a > 0$ (positive if $b/a < 0$, negative if $b/a > 0$).

Each Δ_j is a function of $T, k_e, C_2, C_5, C_s, \alpha, Z_m$ and Z_s but not a function of C_3 or C_6 as the last two parameters only appear in the numerator of (5). Therefore conditions (20) determine the space of stabilising controllers, sampling time and environment stiffness for given master and slave inertias. In addition, for practical reasons, we impose the following conditions on the control parameters C_2 and C_5 :

- The force feedback gain C_2 should be non-negative, otherwise the direction of the reflected force will be wrong

$$C_2 \geq 0 \quad (21)$$

- The slave local feedback gain C_5 should be non-positive as a measure to counteract the environment force f_e but it should not be less than -1 (note the term $-(1 + C_5)f_e$ in the control effort of the slave in Fig. 2)

$$-1 \leq C_5 \leq 0 \quad (22)$$

Each Δ_j is a polynomial of order $j - 1$ in k_e . Therefore for given master and slave inertias and to have stable teleoperation, conditions (20) set lower and upper bounds on the environment stiffness as

$$\gamma_1 \leq k_e \leq \gamma_2 \quad (23)$$

where γ_1 and γ_2 are functions of the control gains and the sampling time. With regard to (23), two points should be considered:

- It is desirable to have

$$\gamma_2 \rightarrow +\infty \quad (24)$$

to have maximum stability robustness against variations in k_e .

- It is imperative to have

$$\gamma_1 = 0 \quad (25)$$

otherwise the teleoperation system would not be stable when the slave is in free space.

It turns out that $i = 3$ and $i = 5$ in (18), which correspond to $n = 4$ and $n = 6$ in (20) respectively, lead to an almost identical lower bound γ_1 , thus we proceed with $i = 3$ for less complexity. Each Δ_j has a factor $k_p^j [C_2 + \alpha(1 + C_5)]^j$ in its denominator. Therefore knowing that $k_p > 0$ (Appendix 2), we must have

$$C_2 + \alpha(1 + C_5) > 0 \quad (26)$$

in order to prevent abrupt sign changes in $\Delta_j, j = 1, \dots, 4$. Otherwise, an infinitesimal change in C_2 or C_5 such that $C_2 + \alpha(1 + C_5)$ crosses zero causes the terms of odd order (Δ_1 and Δ_3) to change sign and destabilises the system. Fortunately, (26) is ensured due to constraints (21) and (22) that we have already assumed for C_2 and C_5 .

In the rest of this section, we derive additional conditions for having $\Delta_j > 0$ for each j . Without loss of generality, since we are only concerned about conditions for stability, we assume strict inequalities. Replacing inequalities by equalities in the stability conditions that will follow gives the borderline of stability and instability.

5.1 $j = 1$

The expression for Δ_1 is independent of k_c and $\Delta_1 > 0$ imposes the following lower bound on k_{v_s}

$$k_{v_s} > \varphi_1(T, k_{p_s}, C_i, \alpha) = k_{p_s} T \left(1 - \frac{\alpha/2}{C_2 + \alpha(1 + C_5)} \right) \quad (27)$$

or, alternatively, the following upper bound on T

$$T < \zeta_1(k_{v_s}, k_{p_s}, C_i, \alpha) = \frac{k_{v_s}}{k_{p_s} (1 - (\alpha/2)/(C_2 + \alpha(1 + C_5)))} \quad (28)$$

5.2 $j = 2$

The expression for Δ_2 involves k_c^{-1}

$$\Delta_2 = Q_2(M_2 + N_2/k_c) \quad (29)$$

where M_2 and N_2 are functions of the control and system parameters and the sampling time, and Q_2 is a positive term. Assuming $T^2, T^3 \simeq 0$ for mathematical simplicity, the solution to $\Delta_2 = 0$ is

$$k_{e0} = \frac{-N_2}{M_2} = \frac{Tk_{p_s}^2 (M_m + \alpha M_s)(C_2 + \alpha C_5)}{m_2 k_{v_s}^2 + n_2 k_{v_s} + p_2} \quad (30)$$

where

$$\begin{aligned} m_2 &= -2T[C_2 + \alpha(1 + C_5)][C_2 + \alpha(C_5 + 1/2)] \\ n_2 &= 2M_m(1 + C_5)[C_2 + \alpha(1 + C_5)] \\ p_2 &= -TM_m k_{p_s} [(1 + C_5)(C_2 + \alpha(1 + C_5)) + C_2] \end{aligned}$$

Because of (21), (22) and (26), we have $n_2 > 0$ and $p_2 < 0$. Also, as will be seen later, for the case $j = 3$, $\Delta_3 > 0$ requires that

$$C_2 + \alpha C_5 < 0 \quad (31)$$

implying that $N_2 > 0$.

In order to ensure (25), it is necessary that $k_{e0} < 0$ (because if Δ_2 changes sign at a positive k_c , then (25) would be violated). To this end, since $N_2 > 0$, M_2 needs to be positive. To find the conditions under which $M_2 > 0$, we distinguish the following four cases:

- *Case 1:* $m_2 < 0$ and $n_2^2 - 4m_2 p_2 < 0$. The quadratic polynomial M_2 will never be positive for any k_{v_s} , and therefore this case is not of interest.
- *Case 2:* $m_2 < 0$ and $n_2^2 - 4m_2 p_2 \geq 0$. Since $n_2 > 0$ and $p_2 < 0$, $M_2 = 0$ has two real positive solutions implying that $M_2 < 0$ holds only if k_{v_s} is between these two solutions.
- *Case 3:* $m_2 > 0$ and $n_2^2 - 4m_2 p_2 < 0$. This is impossible because we know $p_2 < 0$.

- *Case 4:* $m_2 > 0$ and $n_2^2 - 4m_2 p_2 \geq 0$. Since $n_2 > 0$ and $p_2 < 0$, $M_2 = 0$ has one real positive and one real negative solution and $M_2 > 0$ holds if k_{v_s} (positive, according to Appendix 2) is greater than the positive root.

Similar to a discretely simulated virtual wall [conditions (1) and (2)], Case 2 is not opted for as an upper bound on k_{v_s} is not desirable. Consequently, Case 4 (whereby M_2 has one real positive and one real negative root) is the only possibility for ensuring $M_2 > 0$ and therefore (25), resulting in the following two conditions

$$C_2 + \alpha(C_5 + 1/2) < 0 \quad (32)$$

$$k_{v_s} > \varphi_2(T, k_{p_s}, C_i, \alpha, M_m) = \max\{\text{Root}(M_2)\} \quad (33)$$

In the above discussion, to ensure $M_2 > 0$, a lower bound on k_{v_s} was imposed. Alternatively, an upper bound on T can be derived to fulfil $M_2 > 0$. To this end, note that $M_2' = m_2' T + n_2' > 0$ where, because of (32), $m_2' = (m_2 k_{v_s}^2 + p_2)/T < 0$ and $n_2' = n_2 k_{v_s} > 0$. Therefore (33) and the following upper bound on T have the same effect

$$T < \zeta_2(k_{v_s}, k_{p_s}, C_i, \alpha, M_m) = -\frac{n_2'}{m_2'} \quad (34)$$

5.3 $j = 3$

We have

$$\Delta_3 = Q_3(M_3 + N_3/k_c + P_3/k_c^2) \quad (35)$$

where $Q_3 > 0$. Assuming $T^2, \dots, T^6 \simeq 0$, we have

$$\begin{aligned} M_3 &= -M_m^2 T C_5 (1 + C_5) [C_2 + \alpha(1 + C_5)] \\ N_3 &= m_3 k_{v_s}^2 + n_3 k_{v_s} + p_3 \\ P_3 &= -T k_{p_s}^2 (M_m + \alpha M_s)^2 (C_2 + \alpha C_5) \end{aligned}$$

where

$$\begin{aligned} m_3 &= -T(C_2 + \alpha C_5)(M_m + \alpha M_s)[C_2 + \alpha(1 + C_5)] \\ n_3 &= 2M_m [C_2 + \alpha(1 + C_5)] [-C_2 M_s + M_m(1 + C_5)] \\ p_3 &= a_3 (M_m - \alpha M_s)^2 + b_3 (M_m - \alpha M_s) + c_3 \end{aligned} \quad (36)$$

and a_3 and b_3 are functions of the system and control parameters and the sampling time and

$$c_3 = -2T \alpha M_s^2 k_{p_s} [\alpha^2(1 + C_5) - 2C_2(C_2 + \alpha C_5)] \quad (37)$$

Because of (22) and (26), we have $M_3 > 0$. Therefore if $P_3 < 0$, then $N_3^2 - 4M_3 P_3 > 0$ implying that (35) will have a negative and a positive root with respect to k_c . As a result, if $P_3 < 0$, since $M_3 > 0$ the condition $\Delta_3 > 0$ will hold only if k_c is greater than the positive root, amounting

to a non-zero, positive γ_1 in breach of (25). Therefore, we are only interested in $P_3 > 0$, which leads to (31).

Having ensured $P_3 > 0$, we distinguish the following two cases:

- *Case 1:* $N_3^2 - 4M_3P_3 < 0$. In this case, since $M_3 > 0$, the condition $\Delta_3 > 0$ will hold regardless of k_c .
- *Case 2:* $N_3^2 - 4M_3P_3 \geq 0$. In this case, we need $N_3 > 0$ in order to ensure (25). Otherwise, since $M_3 > 0$ and $P_3 > 0$, (35) will have two real positive roots, resulting in a non-zero, positive lower bound on k_c .

The expression $N_3^2 - 4M_3P_3$ can be viewed as a second-order polynomial in T or a fourth-order polynomial in k_{v_s} . In the following, we discuss why Case 1, that is, $N_3^2 - 4M_3P_3 < 0$, is not an option regardless of how it is viewed:

- Implications of $N_3^2 - 4M_3P_3 < 0$ on T : it turns out that $N_3^2 - 4M_3P_3 = m'_3T^2 + n'_3T + p'_3$ where $p'_3 = (n_3k_{v_s})^2 > 0$. We distinguish the following four cases:

– *Case 1:* $m'_3 < 0$ and $n'^2_3 - 4m'_3p'_3 < 0$. This is impossible because we know that $p'_3 > 0$.

– *Case 2:* $m'_3 < 0$ and $n'^2_3 - 4m'_3p'_3 \geq 0$. In this case, since $p'_3 > 0$, the second-order polynomial has one real positive and one real negative solution. In order to have $N_3^2 - 4M_3P_3 < 0$, the sampling period T needs to be greater than the positive root. However, a non-zero lower bound on T is not acceptable because as $T \rightarrow 0$, the discrete-time system approaches the continuous-time system, which was proved stable in Section 3.

– *Case 3:* $m'_3 > 0$ and $n'^2_3 - 4m'_3p'_3 < 0$. In this case, $N_3^2 - 4M_3P_3 < 0$ never happens.

– *Case 4:* $m'_3 > 0$ and $n'^2_3 - 4m'_3p'_3 \geq 0$. In this case, again since $p'_3 > 0$, depending on the sign of n'_3 , the second-order polynomial has either two real negative or two real positive solutions, and $N_3^2 - 4M_3P_3 < 0$ holds if T is between the two solutions. For the negative solutions, this is impossible as $T > 0$ and for the positive solutions, it is unacceptable to put a non-zero lower bound on T .

- Implications of $N_3^2 - 4M_3P_3 < 0$ on k_{v_s} : The coefficient of $k_{v_s}^4$ in $N_3^2 - 4M_3P_3$ is equal to $m^2_3 > 0$. The polynomial can either have four distinct real roots or two distinct real roots and two complex conjugate roots (note that if it has four complex conjugate roots, then $N_3^2 - 4M_3P_3 < 0$ will not hold as the coefficient of $k_{v_s}^4$ is positive; also, note that duplicate real roots do not change the sign of a polynomial). In order to have $N_3^2 - 4M_3P_3 < 0$,

assuming roots $k_{v_{s1}} < k_{v_{s2}} < k_{v_{s3}} < k_{v_{s4}}$, we need either $k_{v_{s1}} < k_{v_s} < k_{v_{s2}}$ or $k_{v_{s3}} < k_{v_s} < k_{v_{s4}}$, in both cases imposing an upper bound on k_{v_s} . Consequently, this case is not of interest as such upper bounds on k_{v_s} should be avoided as far as possible.

In summary, $N_3^2 - 4M_3P_3 < 0$ imposes a lower bound on T and an upper bound on k_{v_s} . Although for specific choices of T and k_{v_s} such bounds may not create difficulties, in a general analysis they need to be avoided for the reasons explained earlier. Therefore because of the unacceptable conditions that $N_3^2 - 4M_3P_3 < 0$ imposes on T and k_{v_s} , we only seek conditions that ensure Case 2, that is, $N_3^2 - 4M_3P_3 \geq 0$ and $N_3 > 0$.

5.3.1 Conditions for ensuring $N_3 > 0$: The expression for N_3 is of second order in k_{v_s} , $N_3 = m_3k_{v_s}^2 + n_3k_{v_s} + p_3$, or of first order in T , $N_3 = m''_3T + n''_3$.

N_3 as a function of k_{v_s} : Noting that $m_3 > 0$ as a result of (26) and (31), we distinguish the following two cases.

- *Case 1:* $n^2_3 - 4m_3p_3 < 0$. In this case, $N_3 > 0$ holds for all values of k_{v_s} , thus no new condition is imposed.

- *Case 2:* $n^2_3 - 4m_3p_3 > 0$. A lower bound equal to the larger root of $N_3 = 0$ will be imposed on k_{v_s} .

In practice, the constant $\alpha = C_m/C_s$ is often chosen to be

$$\alpha = \frac{M_m}{M_s} \tag{38}$$

as the master and the slave control actions need to be proportional to their inertias. This will ensure that the master and the slave have similar closed-loop behaviour. Choosing α according to (38) simplifies p_3 to c_3 and therefore on the basis of (21), (22) and (31), $p_3 < 0$. Also, with (38)

$$n^2_3 - 4m_3p_3 = -4\alpha^2M_s^3[C_2 + \alpha(1 + C_5)]R_3 \tag{39}$$

where

$$\begin{aligned} R_3 &= R'_3k_p T^2 - R''_3 \\ R'_3 &= 4[\alpha^2(1 + C_5) - 2C_2(\alpha C_5 + C_2)](\alpha C_5 + C_2) \\ R''_3 &= M_s[C_2 + \alpha(1 + C_5)][-C_2 + \alpha(1 + C_5)]^2 \end{aligned} \tag{40}$$

Because of (21), (22), (26) and (31), we have $R'_3 < 0$ and $R''_3 > 0$. Therefore $R_3 < 0$ regardless of T and based on (39), Case 1 never happens.

Since $m_3 > 0$, in Case 2, the root of $N_3 = 0$ lower bounds k_{v_s} :

$$k_{v_s} > \varphi_4(T, k_{p_s}, C_i, \alpha, M_m, M_s) = \max\{\text{Root}(N_3)\} \quad (41)$$

Since $m_3 > 0$ and $p_3 < 0$, $N_3 = 0$ has a positive root and therefore in (41), $\varphi_4 > 0$.

$$N_3 \text{ as a function of } T: \text{ If arranged as } N_3 = m_3''T + n_3''$$

$$m_3'' = m_3'''k_{v_s}^2 + n_3''' \quad (42)$$

$$n_3'' = 2\alpha k_{v_s} M_s^2[-C_2 + \alpha(1 + C_5)][C_2 + \alpha(1 + C_5)]$$

where

$$m_3''' = -2\alpha M_s[C_2 + \alpha(1 + C_5)](C_2 + \alpha C_5) \quad (43)$$

$$n_3''' = -2\alpha k_{p_s} M_s^2[\alpha^2(1 + C_5) - 2C_2(C_2 + \alpha C_5)]$$

We need to have $n_3'' > 0$, resulting in

$$-C_2 + \alpha(1 + C_5) > 0 \quad (44)$$

Otherwise, either $N_3 > 0$ is impossible (if $m_3'' < 0$) or imposes a lower bound on T (if $m_3'' > 0$) which is not acceptable as was discussed earlier. Also note that $m_3''' > 0$ and $n_3''' < 0$ as a result of (21), (22), (26) and (31). Having ensured $n_3'' > 0$, we distinguish the following two cases.

- *Case 1:* $m_3'' < 0$. In this case, an upper bound on T (to satisfy $N_3 > 0$) and an upper bound on k_{v_s} (to satisfy $m_3'' < 0$) are simultaneously imposed.

- *Case 2:* $m_3'' > 0$. In this case, no condition on T (to satisfy $N_3 > 0$) and a lower bound on k_{v_s} (to satisfy $m_3'' > 0$) are imposed.

As was discussed earlier, we would like to avoid an upper bound on k_{v_s} as much as possible. Therefore we opt for Case 2, which imposes the following condition on k_{v_2}

$$k_{v_s} > \zeta_3(k_{p_s}, C_i, \alpha, M_s) = \sqrt{\frac{-n_3'''}{m_3'''}} \quad (45)$$

5.3.2 Conditions for ensuring $N_3^2 - 4M_3P_3 \geq 0$:

Since $N_3^2 - 4M_3P_3$ is a fourth-order polynomial in k_{v_s} in which the coefficient of $k_{v_s}^4$ is positive, the following condition is sufficient for $N_3^2 - 4M_3P_3 > 0$

$$k_{v_s} > \varphi_5(T, k_{p_s}, C_i, \alpha, M_m, M_s) \quad (46)$$

where φ_5 is the biggest real root of $N_3^2 - 4M_3P_3$

$$\varphi_5 = \max\{\text{Root}(N_3^2 - 4M_3P_3)\} \quad (47)$$

Again, $N_3^2 - 4M_3P_3$ can be viewed as a second-order polynomial in T leading to a similar constraint involving k_{v_s} and T , which is not discussed here for brevity.

5.4 $j = 4$

While conditions (20) for $j = 1, 2, 3$ imposed conditions on $C_2, C_5, \alpha, T, k_{p_s}$ and k_{v_s} such that the teleoperation system is stable with the slave in free space [i.e. $\gamma_1 = 0$ in (23)], condition $\Delta_4 > 0$ affects both the lower bound γ_1 and the upper bound γ_2 . Therefore we split the discussion into the following two parts.

5.4.1 Slave in free space; $k_e = 0$: While we previously derived lower bounds on k_{v_s} , condition $\Delta_4 > 0$ also puts an upper bound on k_{v_s} . Indeed, excessively high values for k_{v_s} can cause $\Delta_4 < 0$ when $k_e = 0$, jeopardising stability when the slave is in free space. To investigate this issue, assuming $T^3, \dots, T^{10} \simeq 0$, we have

$$\Delta_4|_{k_e=0} = Q_4(M_4k_{v_s}^2 + N_4k_{v_s} + P_4) \quad (48)$$

where $Q_4 > 0$ and

$$M_4 = 256T^2k_{p_s}^2(M_m + \alpha M_s)^3(C_2 + \alpha C_5)$$

$$N_4 = -512TM_mM_s k_{p_s}^2(M_m + \alpha M_s)^2(C_2 + \alpha C_5)$$

$$P_4 = 256T^2M_mM_s k_{p_s}^3(M_m + \alpha M_s)^2(C_2 + \alpha C_5)$$

Therefore based on (31), $M_4 < 0, N_4 > 0$ and $P_4 < 0$. In order to have $\Delta_4|_{k_e=0} > 0$, it is required that $N_4^2 - 4M_4P_4 > 0$, which results in the following condition

$$k_{p_s} T^2 < \varphi_6(\alpha, M_m, M_s) = \frac{M_m M_s}{M_m + \alpha M_s} \quad (49)$$

When (49) holds, (48) has two positive roots, which are the lower and upper bounds on k_{v_s} such that $\Delta_4|_{k_e=0} > 0$

$$\varphi_7 < k_{v_s} < \varphi_8 \quad (50)$$

where

$$\varphi_7 = \min\{\text{Root}(\Delta_4|_{k_e=0})\} \quad (51)$$

$$\varphi_8 = \max\{\text{Root}(\Delta_4|_{k_e=0})\} \quad (52)$$

5.4.2 Slave in contact with an environment; $k_e \neq 0$:

Condition $\Delta_4 > 0$ decides the upper bound on k_e , that is, γ_2 . While taking $i = 3$ or $i = 5$ in (18) yield similar results with respect to γ_1 , using $i = 5$ gives a less conservative (i.e. larger) γ_2 . However, increasing the order of approximation in (15) to $\mathcal{O}(T^8)$ affects γ_2 negligibly. With $i = 5$ in (18) and assuming $T^4, \dots, T^{10} \simeq 0$, we have

$$\Delta_4|_{k_e \neq 0} = R_4'(M_4'k_e^3 + N_4'k_e^2 + P_4'k_e + Q_4') \quad (53)$$

where $R_4' > 0$, and N_4', P_4' and Q_4' are polynomials in k_{v_s} of

orders 3, 4 and 2, respectively. Also

$$M'_4 = \frac{256}{3} T^3 M_m^3 k_{v_s} C_5 (1 + C_5) [C_2 + \alpha(1 + C_5)] \quad (54)$$

On the basis of (22) and (26), $M'_4 < 0$. This means that $k_c \rightarrow \infty$ causes $\Delta_4 < 0$ and thus the system becomes unstable. The upper bound on k_c is obtained as

$$k_c \leq \gamma_2(T, k_{p_s}, k_{v_s}, C_i, \alpha, M_m, M_s) = \max\{\text{Root}(\Delta_4 |_{k_c \neq 0})\} \quad (55)$$

Again, (53) can be viewed as a third-order polynomial in T , which imposes an upper bound on T if k_c and k_{v_s} are given. Also, (53) is a fourth-order polynomial in k_{v_s} imposing lower and upper bounds on k_{v_s} for given T and k_c .

5.5 $j = 5, 6$

As was mentioned earlier, for $i = 3$ in (18), we will have terms up to Δ_4 in (20). For $i = 5$ in (18), there will also be Δ_5 and Δ_6 . However, in this case it can be shown that the previous conditions ensuring $\Delta_1, \dots, \Delta_4 > 0$ also ensure $\Delta_5 > 0$ and $\Delta_6 > 0$, thus no new additional conditions are imposed on the system and control parameters, the sampling time or the environment stiffness.

6 Simulation study

To further investigate the stability and performance of a teleoperation system under discrete-time control, we simulated a general four-channel teleoperation control architecture using SimuLink. The input f_h simulates a human operator pushing the master with a force of 1 N at

$t = 0 \rightarrow 5$ s such that the slave makes contact with the environment, and retracting the master to the original position at $t = 5 \rightarrow 10$ s. This input waveform repeats every 10 s. This input simulates a soft-tissue palpation task, which is used in surgeries to estimate tissue characteristics and whose effectiveness greatly depends on haptic sensations. Since the system is linear time-invariant, any scaling of the input will be linearly reflected at the output. We chose $M_m = M_s = 1$ kg (thus $\alpha = M_m/M_s = 1$), $k_{v_s} = 20$ Ns/m, $k_{p_s} = 100$ N/m (thus $C_m = \alpha C_s = 20s + 100$), $C_2 = 0.2$, $C_5 = -0.75$, and based on (9), $C_6 = C_2 - 1 = -0.8$ and $C_3 = C_5 + 1 = 0.25$. These choices meet the design conditions derived in Section 5 for ensuring stability.

While the control blocks, which are shaded in Fig. 3, were discretised using the Tustin's transformation $s = 2(z - 1)/(T(z + 1))$ and realised using z -domain transfer functions, the rest of the system was implemented using s -domain transfer functions. To enable transfer of data between continuous- and discrete-time blocks, which operate at different rates, rate transition blocks were used for implementation of samplers and ZOHs in Fig. 3. A variable-step, Dormand-Prince (ode45), continuous-time solver was used.

Fig. 4 shows the maximum environment stiffness for a given sampling time such that teleoperation remains stable for the cases of $i = 3$ (i.e. V_3), $i = 5$ (i.e. V_5), and simulations. Fig. 4 can be considered a tradeoff graph as it demonstrates the tradeoff between the contact stiffness and the sampling period. As expected and similar to the case of a discretely simulated virtual wall with stability

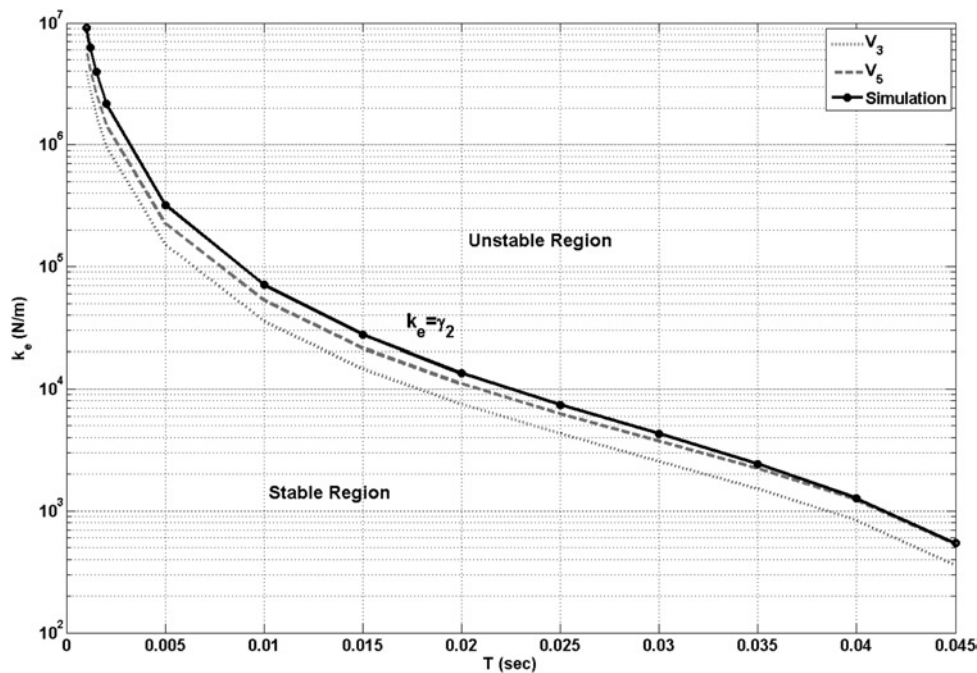


Figure 4 Stability/instability regions in k_e - T plane for $k_{v_s} = 20$ Ns/m

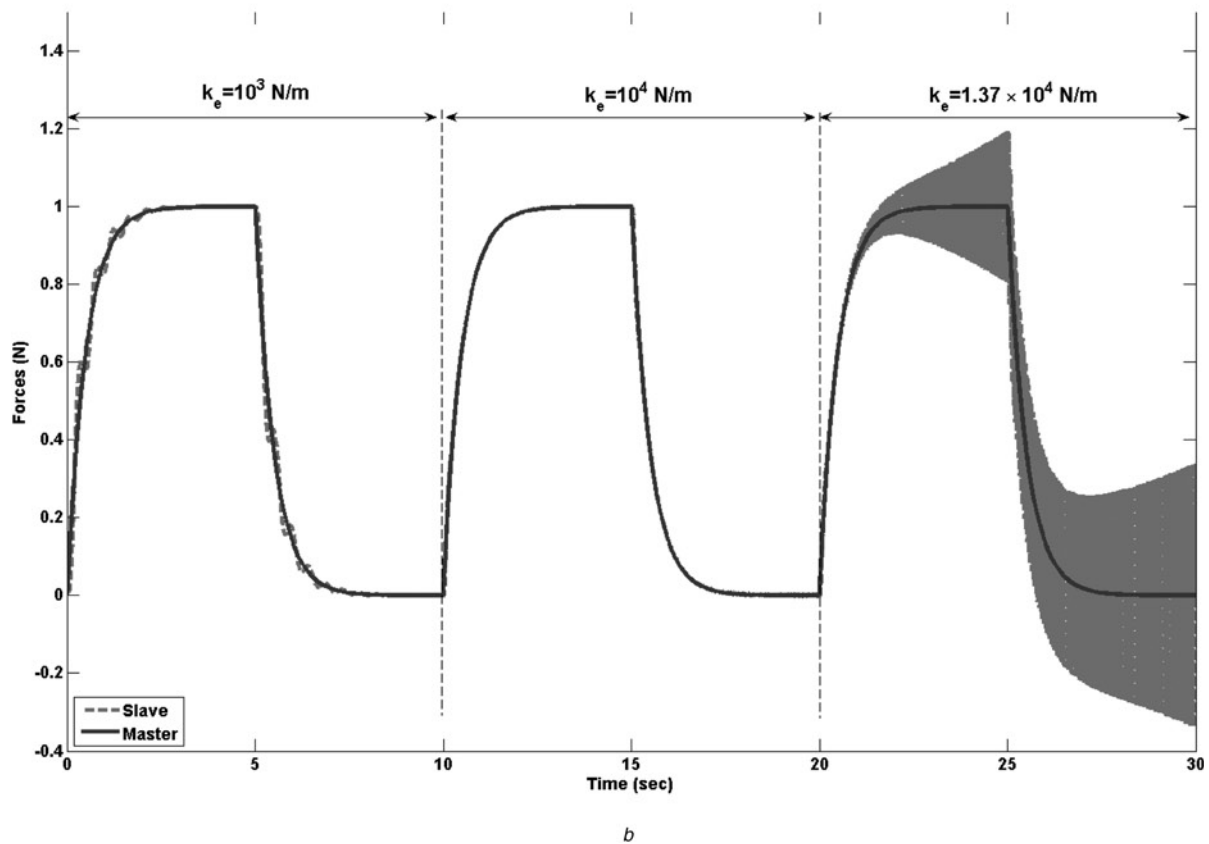
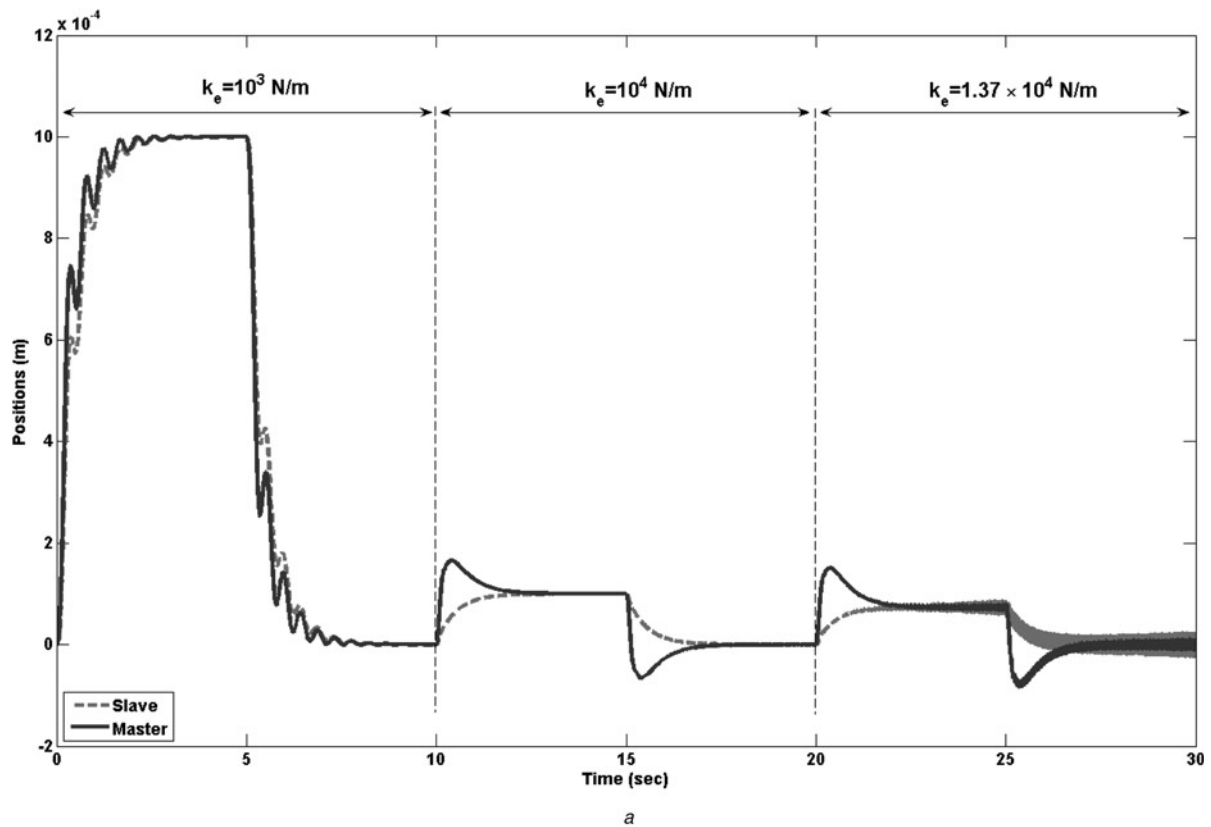
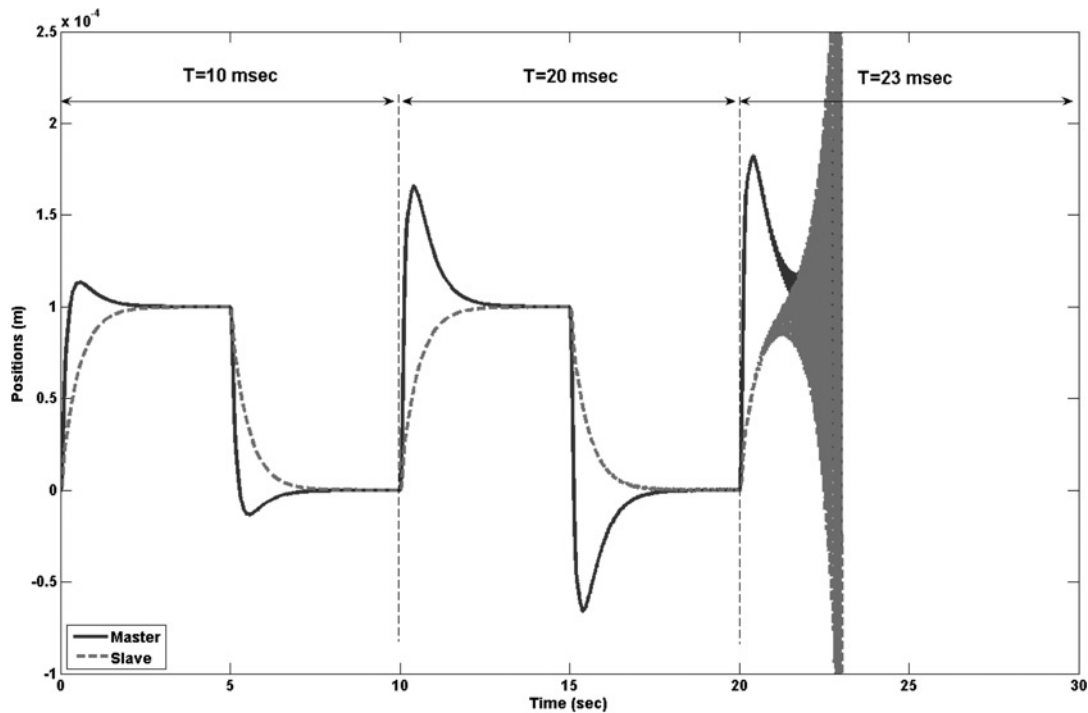


Figure 5 Profiles of positions and forces for the master (solid) and the slave (dashed) when $T = 20$ ms, $k_v = 20$ Ns/m and $k_e = 10^3, 10^4$ and 1.37×10^4 N/m

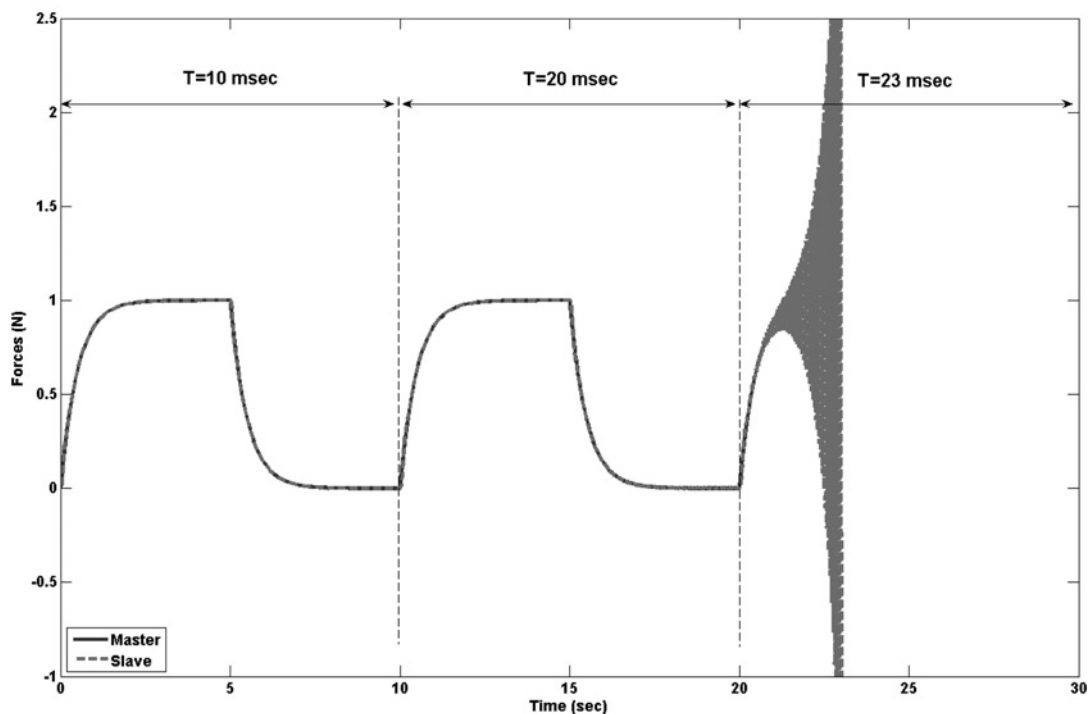
a Position profile
b Force profile

condition (2), higher sampling periods allow for lower maximum environment stiffnesses (k_e can vary from zero up to γ_2). As can be seen, increasing i in (18) from 3 to 5 enhances the precision of the upper bound on k_e given

by (55). It was confirmed by both analysis and simulation that further increase in i to 7 or 9 has a negligible effect on the precision of γ_2 (the obtained curves coincide with that of $i = 5$).



a



b

Figure 6 Profiles of positions and forces for the master (solid) and the slave (dashed) when $k_e = 10^4$ N/m, $k_v = 20$ Ns/m and $T = 10, 20$ and 23 ms

a Position profile
b Force profile

When $i = 5$, the order of precision of the differentiation method affects the accuracy of γ_2 as given by (55). For instance, it was observed that using $s = T/(z - 1)$ or $s = Tz/(z - 1)$ (based on backward- and forward-rectangular integration) instead of $s = 2(z - 1)/(T(z + 1))$ (based on trapezoidal integration) in determining (17) drives γ_2 very distant from the simulation results. In fact, increasing the order of precision of differentiation reduces the distance between the theoretical and the simulation results at the cost of higher computational complexity and less mathematical tractability.

Fig. 5 shows the master and the slave position and force profiles for $T = 20$ ms and $k_{v_s} = 20$ Ns/m. As expected, with an increase in the environment stiffness from $k_c = 10^3$ N/m to $k_c = 10^4$ N/m, the master and the slave peak positions are reduced to a tenth as the operator's input force profile remains the same. As can be seen, the teleoperation system is stable for $k_c = 10^3$ N/m and 10^4 N/m but is unstable for $k_c = 1.37 \times 10^4$ N/m. This result was to be expected from the stability/instability regions of Fig. 4.

Fig. 6 shows the same profiles for $k_c = 10^4$ N/m and $k_{v_s} = 20$ Ns/m. As can be seen, as T is increased from $T = 10$ ms to 20 ms, the master's position response becomes underdamped as the effective damping introduced by the controller is reduced [$k_{v_s}s = k_{v_s}(2(z - 1)/(T(z + 1)))$]. With regard to stability, as expected based on the regions of stability and instability shown in Fig. 4, the

teleoperation system is stable for $T = 10$ ms and 20 ms but not for 23 ms.

Fig. 7 illustrates the effect of the damping introduced by the controller on the maximum allowable sampling period for a typical environment stiffness $k_c = 1000$ N/m (the same simulation parameters as before were used). Fig. 7 can be considered a design graph as it has the two main control design parameters (T and k_{v_s}) as its coordinates. From (50), the stabilising range of k_{v_s} for $k_c = 0$ is $0 < k_{v_s} < 200$. As can be seen in Fig. 7, added damping up to $k_{v_s} = 6.8$ has a constructive effect on system robust stability while further increase in damping reduces the maximum allowable sampling period. Simulation results precisely match the theoretical results of Fig. 7 for $T \leq 49$ ms and therefore they are not shown separately on this figure. For $T > 49$ ms, the fact that high orders of T were ignored during the stability analysis for less complexity causes some discrepancy between the simulation results and the outcome of the theoretical analysis.

Fig. 8 shows the master and the slave positions and forces for $k_c = 10^3$ N/m and $T = 20$ ms. As expected, with an increase in the damping introduced by the controller from $k_{v_s} = 3$ Ns/m to 10 Ns/m, the master and the slave responses are much less oscillatory. As can be seen, consistent with the stability/instability regions of Fig. 7, the teleoperation system is stable for $k_{v_s} = 10$ Ns/m but becomes unstable for $k_{v_s} = 3$ Ns/m and 48.7 Ns/m.

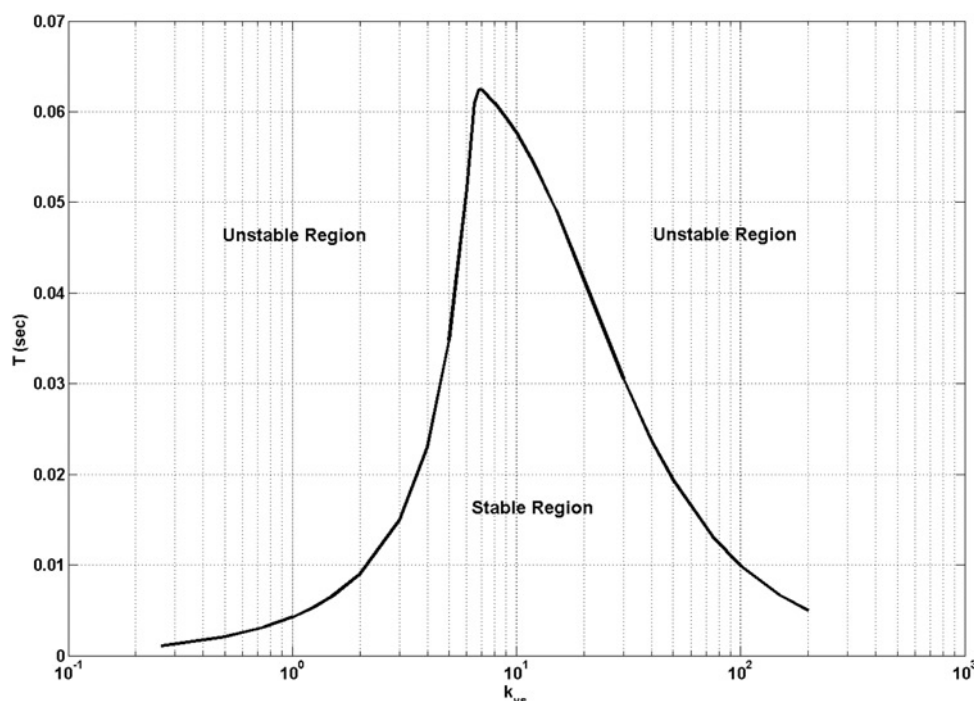
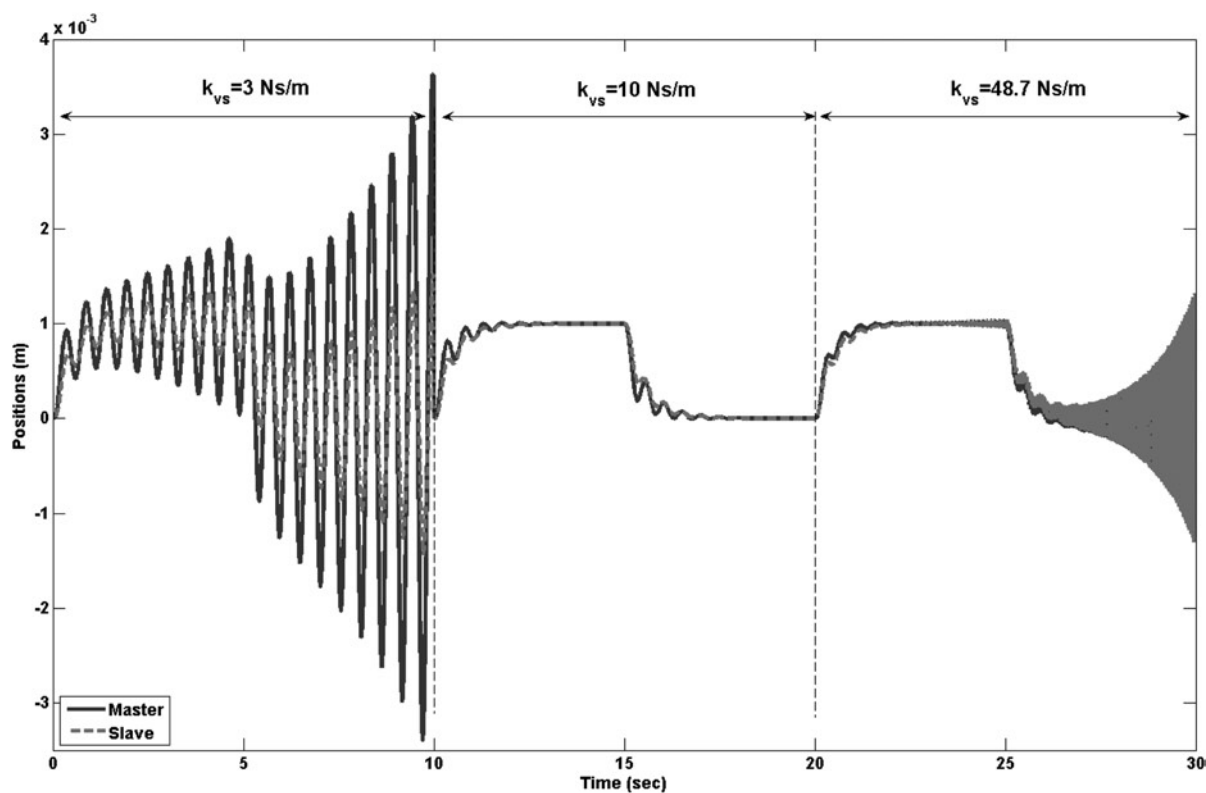
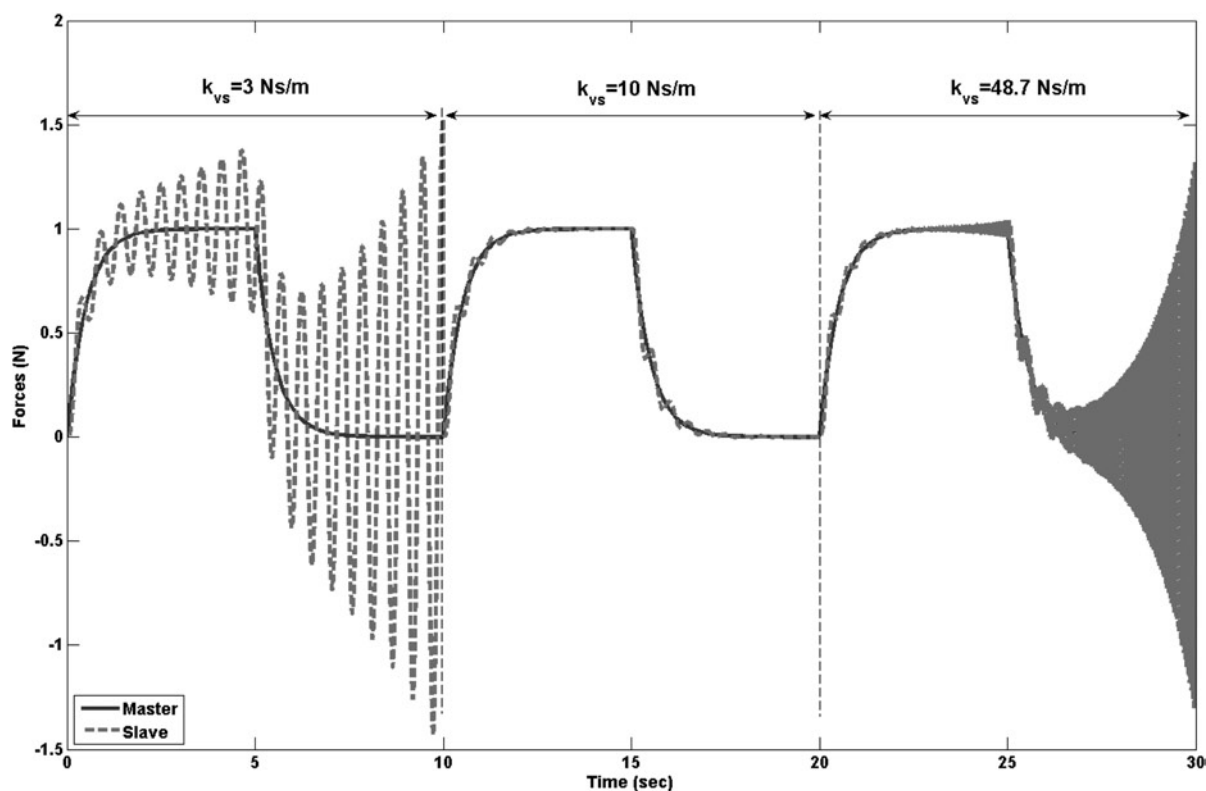


Figure 7 Stability/instability regions in T - k_{v_s} plane for $k_e = 1000$ N/m



a



b

Figure 8 Profiles of positions and forces for the master (solid) and the slave (dashed) when $k_e = 10^3 \text{ N/m}$, $T = 20 \text{ ms}$ and $k_{vs} = 3, 10 \text{ and } 48.7 \text{ Ns/m}$

a Position profile
b Force profile

7 Conclusions

Issues with the stability of teleoperation can arise when a bilateral controller designed in the continuous-time domain is converted into the discrete-time domain. In this paper, first the hybrid model of a digitally controlled four-channel teleoperation system was derived. Next, without making any assumptions about human operator dynamics, regions of stability of the discrete-time-controlled teleoperation system were obtained in the form of conditions on the control parameters, sampling period and environment stiffness. Specifically, requirements on the control parameters (notably, lower and upper bounds on the controller damping) and upper bounds on the sampling period and environment stiffness were derived such that stability of the teleoperation system under discrete-time bilateral control is ensured. It was found that as the sampling period is increased, the maximum admissible stiffness of the environment with which a slave robot can stably interact is reduced. The result is a set of design guidelines in terms of various digital control parameters and the sampling rate for stable teleoperation, especially when interacting with a rigid environment. The theoretical results obtained from the stability analysis were confirmed by a simulation study in which the bilateral controller was realised by z -domain transfer functions, whereas the master, the slave and the environment were simulated in the s -domain. Lastly, friction dissipates energy and plays a stabilising role in a teleoperation system. Therefore the stability regions found in this paper correspond to a worst-case scenario.

8 Acknowledgments

This research was supported by the Natural Sciences and Engineering Research Council (NSERC) of Canada under grants RGPIN-1345 and RGPIN-227612, and infrastructure grants from the Canada Foundation for Innovation awarded to the London Health Sciences Centre (CSTAR) and the University of Western Ontario (R.V. Patel).

9 References

- [1] LAWRENCE D.A.: 'Stability and transparency in bilateral teleoperation', *IEEE Trans. Robot. Autom.*, 1993, **9**, pp. 624–637
- [2] HER M.G., HSU K.S., YU W.S., KARKOUB M.: 'Analysis and design of haptic telerobotic system', *IEE Proc., Control Theory Appl.*, 2001, **148**, pp. 306–314
- [3] ISTEPANIAN R.S.H., WU J., WHIDBORNE J.F., YAN J., SALCUDEAN S.E.: 'Finite word length stability issues of a teleoperation motion-scaling control system'. UKACC Int. Conf. Control, 1998, vol. 2, pp. 1676–1681
- [4] NIEMEYER G., SLOTINE J.J.E.: 'Telemanipulation with time delays', *Int. J. Robot. Res.*, 2004, **23**, (9), pp. 873–890
- [5] ARCARA P., MELCHIORRI C.: 'Control schemes for teleoperation with time delay: a comparative study', *Robot. Auton. Syst.*, 2002, **38**, pp. 49–64
- [6] SOEDA M., WARWICK K., CRADDOCK R.J., FURUYA T.: 'Human-computer cooperative teleoperation with time delay'. UKACC Int. Conf. Control, 1998, vol. 2, pp. 1444–1449
- [7] MUNIR S., BOOK W.J.: 'Internet-based teleoperation using wave variables with prediction', *IEEE/ASME Trans. Mechatronics*, 2002, **7**, (2), pp. 124–133
- [8] NI L., WANG D.W.L.: 'A gain-switching control scheme for position-error-based bilateral teleoperation: contact stability analysis and controller design', *Int. J. Robot. Res.*, 2004, **23**, (3), pp. 255–274
- [9] MAHVASH M., OKAMURA A.M.: 'Friction compensation for a force-feedback telerobotic system'. Proc. IEEE Int. Conf. Robotics and Automation, Orlando, FL, 2006, pp. 3268–3273
- [10] BERESTESKY P., CHOPRA N., SPONG M.W.: 'Discrete time passivity in bilateral teleoperation over the Internet'. Proc. Int. Conf. Robotics and Automation, New Orleans, LA, 2004, pp. 4557–4564
- [11] HIRCHE S.: 'Haptic telepresence in packet switched communication networks' (Technical University of Munich, Munich, Germany, 2005)
- [12] GILLESPIE R.B., CUTKOSKY M.: 'Stable user-specific rendering of the virtual wall'. Proc. ASME Int. Mechanical Engineering Conf. and Exposition, Atlanta, GA, 1996, vol. 58, pp. 397–406
- [13] LEUNG G.M.H., FRANCIS B.A.: 'Bilateral control of teleoperators with time delay through a digital communication channel'. Proc. 30th Annual Allerton Conf. Communication, Control and Computing, 1992, pp. 692–701
- [14] ANDERSON R.J.: 'Building a modular robot control system using passivity and scattering theory'. Proc. IEEE Int. Conf. Robotics and Automation, Minneapolis, MN, 1996, vol. 1, pp. 698–705
- [15] SECCHI C., STRAMIGIOLI S., FANTUZZI C.: 'Digital passive geometric telemanipulation'. Proc. IEEE Int. Conf. Robotics and Automation, Taipei, Taiwan, 2003, pp. 3290–3295
- [16] STRAMIGIOLI S., SECCHI C., VAN DER SCHAFT A.J., FANTUZZI C.: 'A novel theory for sample data system passivity'. Proc. IEEE/RSJ Int. Conf. Intelligent Robots and Systems, Lausanne, Switzerland, 2002, pp. 1936–1941
- [17] COLGATE J.E., SCHENKEL G.G.: 'Passivity of a class of sampled-data systems: application to Haptic interfaces', *J. Robot. Syst.*, 1997, **14**, (1), pp. 37–47

[18] MILLER B.E., COLGATE J.E., FREEMAN R.A.: 'Guaranteed stability of haptic systems with nonlinear virtual environments', *IEEE Trans. Robot. Autom.*, 2000, **16**, (6), pp. 712–719

[19] MAHVASH M., HAYWARD V.: 'High-fidelity passive force-reflecting virtual environments', *IEEE Trans. Robot.*, 2005, **21**, (1), pp. 38–46

[20] ABBOTT J.J., OKAMURA A.M.: 'Effects of position quantization and sampling rate on virtual wall passivity', *IEEE Trans. Robot.*, 2005, **21**, (5), pp. 952–964

[21] DIOLAITI N., NIEMEYER G., BARBAGLI F., SALISBURY J.K. JR.: 'Stability of haptic rendering: discretization, quantization, time delay and Coulomb effects', *IEEE Trans. Robot.*, 2006, **22**, (2), pp. 256–268

[22] LOVE L., BOOK W.: 'Contact stability analysis of virtual walls'. Proc. ASME Int. Mechanical Engineering Conf. and Exposition, 1995, vol. 57, pp. 689–694

[23] GIL J.J., AVELLO A., RUBIO A., FLOREZ J.: 'Stability analysis of a 1 DOF haptic interface using the Routh–Hurwitz criterion', *IEEE Trans. Control Syst. Technol.*, 2004, **12**, (4), pp. 583–588

[24] GIL J.J., SANCHEZ E., HULIN T., PREUSCHE C., HIRZINGER G.: 'Stability boundary for haptic rendering: influence of damping and delay'. IEEE Int. Conf. Robotics and Automation, Rome, Italy, 2007, pp. 124–129

[25] HASSER C.J.: 'The effects of displacement quantization and zero-order hold on the limit cycle behavior of haptic knobs' (Stanford University, 2001)

[26] SHEN X., GOLDFARB M.: 'On the enhanced passivity of pneumatically actuated impedance-type haptic interfaces', *IEEE Trans. Robot.*, 2006, **22**, (3), pp. 470–480

[27] HASHTRUDI-ZAAD K., SALCUDEAN S.E.: 'Analysis of control architectures for teleoperation systems with impedance/admittance master and slave manipulators', *Int. J. Robot. Res.*, 2001, **20**, (6), pp. 419–445

[28] HAYKIN S.S.: 'Active network theory' (Addison-Wesley, Reading, MA, 1970)

[29] COLGATE J.E.: 'Robust impedance shaping telemanipulation', *IEEE Trans. Robot. Autom.*, 1993, **9**, (4), pp. 374–384

10 Appendix 1: absolute stability theorems

10.1 Llewellyn's criterion

The necessary and sufficient conditions [28] for absolute stability of the teleoperation system (4) are: (a) $h_{11}(s)$ and

$h_{22}(s)$ have no poles in the RHP, (b) any poles of $h_{11}(s)$ and $h_{22}(s)$ on the imaginary axis are simple with real and positive residues and (c) for $s = j\omega$ and all real values of ω the following conditions hold

$$\Re(h_{11}) \geq 0 \quad (56)$$

$$\Re(h_{22}) \geq 0 \quad (57)$$

$$2\Re(h_{11})\Re(h_{22}) - \Re(h_{12}h_{21}) - |h_{12}h_{21}| \geq 0 \quad (58)$$

where $\Re(\cdot)$ and $|\cdot|$ denote the real and absolute values.

10.2 Scattering matrix analysis

The necessary and sufficient condition [29] for absolute stability of a reciprocal two-port network ($S_{12} = S_{21}$) with an RHP-analytic scattering matrix $S(s)$ is

$$\bar{\sigma}[S(j\omega)] \leq 1 \quad (59)$$

where $\bar{\sigma}$ represents the maximum singular value of $S(j\omega)$. In the case of a non-reciprocal two-port network ($S_{12} \neq S_{21}$), the passivity condition (59) is only a sufficient condition for stability.

11 Appendix 2: absolute stability of PEB system

The hybrid matrix for the PEB teleoperation architecture is given by

$$H = \begin{bmatrix} Z_m + C_m \frac{Z_s}{Z_{ts}} & \frac{C_m}{Z_{ts}} \\ -\frac{C_s}{Z_{ts}} & \frac{1}{Z_{ts}} \end{bmatrix} \quad (60)$$

With regard to Llewellyn's criterion, the characteristic polynomial for h_{11} and h_{22} is $M_s s^2 + k_{v_s} s + k_{p_s}$, which has no RHP poles if $k_{v_s}, k_{p_s} > 0$. With respect to (56) and (57), we have

$$\Re(h_{11}) = \frac{M_s(k_{v_s} k_{p_m} - k_{v_m} k_{p_s} + M_s k_{v_m} \omega^2)}{k_{v_s}^2 + (-k_{p_s}/\omega + M_s \omega)^2} \quad (61)$$

$$\Re(h_{22}) = \frac{k_{v_s}}{k_{v_s}^2 + (-k_{p_s}/\omega + M_s \omega)^2} \quad (62)$$

which are non-negative if $k_{v_m}, k_{v_s} > 0$ and

$$k_{v_s} k_{p_m} - k_{v_m} k_{p_s} = 0 \quad (63)$$

Also, the equality to zero in condition (58) holds if (63) holds and $k_{v_m}, k_{p_m} > 0$. Therefore a sufficient condition for absolute stability of the PEB teleoperation system is that $k_{v_m}, k_{p_m}, k_{v_s}, k_{p_s} > 0$ and $C_m(s)/C_s(s) = \alpha$ where α is a non-negative constant.